Electrochimica Acta 197 (2016) 228–240

Contents lists available at ScienceDirect

Electrochimica Acta

journal homepage: www.elsevier.com/locate/electacta

Electrochemical deposition of zeolitic imidazolate framework electrode coatings for supercapacitor electrodes

Stephen D. Worrall[a], Haydn Mann[a], Adam Rogers[a], Mark A. Bissett[b], Martin P. Attfield[a,*], Robert A.W. Dryfe[b,*]

[a] Centre for Nanoporous Materials, School of Chemistry, University of Manchester, Oxford Road, Manchester M13 9PL, United Kingdom
[b] School of Chemistry, University of Manchester, Oxford Road, Manchester M13 9PL, United Kingdom

ARTICLE INFO

Article history:
Received 18 September 2015
Received in revised form 19 February 2016
Accepted 22 February 2016
Available online 24 February 2016

Keywords:
Modified electrodes
metal-organic frameworks
electrochemical growth
supercapacitors

ABSTRACT

Zn and Co electrodes have been successfully coated with five different zeolitic imidazolate frameworks ZIFs (ZIF-4, ZIF-7, ZIF-8, ZIF-14 and ZIF-67) via the anodic dissolution method. Careful control of the reaction conditions allows for electrode coating growth; in contrast to previous reports of electrochemical ZIF growth, which have not succeeded in obtaining ZIF electrode coatings. Coating crystallinity is also shown to be heavily dependent upon reaction conditions, with amorphous rather than crystalline material generated at shorter reaction times and lower linker concentrations. Electrochemical applications for ZIF-coated electrodes are highlighted with the observation of an areal capacitance of 10.45 mF cm^{-2} at 0.01 V s^{-1} for additive-free ZIF-67 coated Co electrodes. This is superior to many reported metal organic framework (MOF)/graphene composites and to capacitance values previously reported for additive-free MOFs.

1. Introduction

Metal-Organic Frameworks (MOFs) are nanoporous materials consisting of individual metal ions, or metal containing inorganic clusters, co-ordinated by the heteroatoms of organic molecules known as linkers [1]. These linkers co-ordinate multiple metal ions, or metal-containing inorganic clusters, to produce a framework structure containing a network of pores in one, two or three dimensions [1]. Ever since MOFs were first conceptualised [2] there has been great interest in the potential applications of their nanoporosity, however it was not until a MOF capable of maintaining its porosity in the absence of guest molecules was reported that assessment of MOFs for potential applications could begin [3]. Specific applications described to date include the use of MOFs as catalysts [4,5] and as catalyst supports [6–8], for gas separation [9–11] and storage [12–14], for drug delivery [15–17] and chromatography [18]. Powders of MOFs acquired by the standard solvothermal synthetic techniques are sufficient for these applications, but for many applications the MOF is preferred in the form of a coating. Biofilm inhibitors[19], sensors [20–23], photonic antennae [24], nanostructure electrodeposition templates [25], supercapacitors [26–33] and electronic, optoelectronic [34] and information storage devices [35,36] are all promising applications which share this requirement.

A variety of non-electrochemical methodologies have been developed to obtain MOFs as coatings which include the seeding method [37–39], the molten linker method [40], electroless metal oxidation [41,42], self-assembled monolayers (SAMs) [43–45], SAMs with Liquid Phase Epitaxy (LPE) [46–48], SAMS with atomic force microscopy nanografting [49],LPE with digital microfluidics [50], LPE with Langmuir- Blodgett film growth [51], UV lithography and imprinting [52], colloidal chemical solution deposition [53], microwave assisted synthesis [54], lithographically controlled wetting and evaporation [55] and pen type lithography [56,57]. Many of these processes are effective in obtaining coatings but require either high temperatures, in the cases of the molten linker method and electroless metal oxidation, excessively long synthesis times in the case of the seeding, SAM, LPE and colloidal methods or require specialised equipment such as UV or pen type lithography set ups.

Electrochemical techniques, in contrast, enable good quality coatings to be obtained at low temperature, with short reaction times and without specialised equipment. The only real limitation is that the growth substrates must be conductive, however this is also a potential advantage as the ability to obtain MOF coatings directly on electrodes could permit their applications in electrochemical energy storage to be studied more readily.

* Corresponding authors. Fax: +44 161 275 4598.
E-mail addresses: m.attfield@manchester.ac.uk (M.P. Attfield), robert.dryfe@manchester.ac.uk (R.A.W. Dryfe).

http://dx.doi.org/10.1016/j.electacta.2016.02.145

There are two main electrochemical methods for obtaining MOFs as coatings which can be broadly described as cathodic and anodic. In the cathodic method both the metal cation and linker species are present in the electrolyte solution. Electrochemical reduction of a pro-base generates a base, which goes on to reduce water to produce a high pH environment local to the cathode surface [58,59]. A high pH environment can promote MOF formation; basic solutions of trialkylamines are often added in traditional solvothermal syntheses. High pH favours MOF formation as it increases the equilibrium concentration of the deprotonated, anionic form of the linker, which interacts with the cationic metal species to produce the MOF. As the high pH environment generated in the cathodic electrochemical method is local to the cathode surface, formation of a MOF coating is favoured over formation of bulk MOF in solution [58,59]. Recent work by the same group has further expanded upon this mechanistic understanding [60] and the method has allowed for the production of coatings of Zn [58–60], Eu [21], Tb [23] and Zr [61] MOFs via this method.

Conversely in the anodic method only the linker species is present in the electrolyte solution; electrochemical oxidation of the metallic anode provides the source of metal cations for the MOF formation [62]. Having originally been developed as a method for bulk solution synthesis of MOFs [62] it was discovered that, dependent upon the reaction conditions, formation of a MOF coating on the anode could be favoured and used to coat defined electrode architectures [63,64]. Utilising this methodology, and in some cases incorporating minor modifications such as the use of galvanic displacement [65] or a high temperature, high pressure (HTHP) cell [19], coatings of Cu [63–66], Fe [19], Tb[22], Gd[22], Zn [67] and Zr [61] MOFs have been obtained. However attempts to synthesise Al MOFs and Zn Zeolitic Imidazolate Frameworks (ZIFs) as coatings via this methodology failed, with the material forming instead exclusively in solution [68]. This was attributed to the larger induction times for the synthesis of these materials, which favours homogenous solution growth over heterogeneous electrode surface growth [68].

ZIFs are a subset of MOFs that are so named due to the topologies they adopt being found in zeolites and the linkers used in their syntheses all being imidazole derivatives [69]. Obtaining ZIF coatings electrochemically is of interest as for many of the previously reported applications for MOF coatings stability to temperature, humidity and a variety of solvents is needed and ZIFs, unlike many of the MOFs made as electrochemical coatings to date, meet these requirements [69]. Combining these useful properties of ZIFs, with the previously mentioned advantages of the electrochemical methods for obtaining MOFs as coatings, is therefore an attractive proposition. Additionally there are over 150 reported ZIFs so far with a wide range of pore sizes and properties which further increase their attractiveness as coatings [70]. With a single exception, where a complicated indirect bipolar electrodeposition modification was used to obtain Zn ZIF-8 [71], no ZIFs have to date been synthesised as coatings electrochemically.

Recently there has been increasing interest in MOFs, particularly ZIFs, as materials for supercapacitor electrodes due to their intrinsically high surface areas, which should be ideal for the storage of charge in the electrical double layer. However due to the low electrical conductivity of most MOFs, in all cases reported hitherto conductive additives were used (such as graphene, graphene oxide, polyaniline or carbon black) or the MOF was pyrolysed to give porous carbons or metal oxides [26–32]. One report combined ZIF-67 with polyaniline to obtain exceptionally high areal capacitance values, however without the polymer additive the value was three orders of magnitude lower [27]. The much greater extent of integration between the MOF and the electrode surface provided by the anodic growth method, as compared to the dispersion of MOF crystals onto electrode surfaces, should mitigate the need for conductive additives and give rise to higher “pure” MOF based capacitance values.

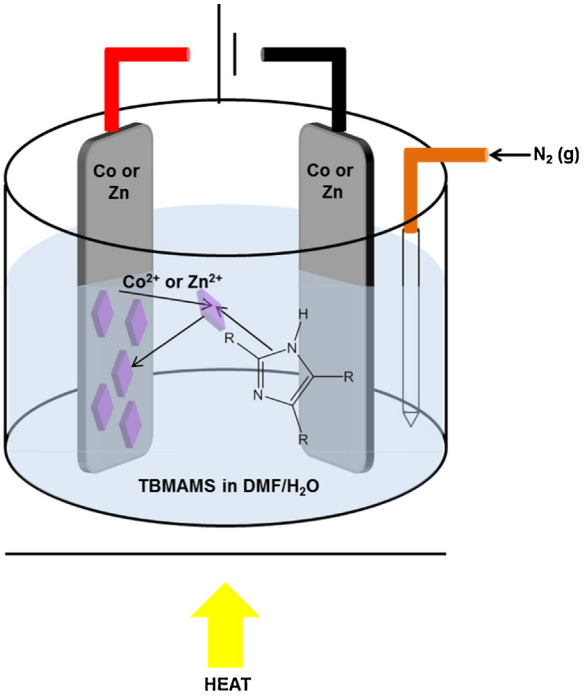

Scheme 1. Illustration of the experimental setup used to synthesise the ZIF coatings. Two Co or Zn electrodes are immersed in a tributylmethylammonium methyl sulphate (TBMAMS) in N, N-dimethylformamide (DMF):H_2O electrolyte solution containing an imidazolate linker. Heat is applied whilst deaerating the solution with N_2(g) and the 2.5 V applied potential difference generates the ZIF coating on the anode.

Here we present the successful electrochemical synthesis of five ZIF coatings via the anodic method encompassing two metals, Zn and Co, and four linkers, imidazole (IM), benzimidazole (bIM), 2-methylimidazole (mIM) and 2-ethylimidazole (eIM). The identity of the coatings is confirmed by powder X-ray diffraction (PXRD), the morphology and quality of the ZIF coatings is analysed by SEM, and the apparent Brunauer-Emmett-Teller (BET) surface area is compared against literature values using N_2(g) adsorption. We demonstrate how careful control of the synthesis conditions enables us to overcome the issue of the separation of the nucleation and growth processes and that it is possible to obtain topologies other than the most thermodynamically stable for a given metal linker combination, increasing the potential of the anodic method for generating a wide variety of thermally and chemically stable porous ZIF coatings. Finally we demonstrate the potential advantage of the anodic dissolution method for obtaining MOF coatings for electrochemical applications, utilising the Co and mIM example, by utilising them as supercapacitor electrodes.

2. Experimental

2.1. Materials

Co foil (99.9%) and Zn foil (99.9%) were obtained from Advent Research Materials. IM (99%) was obtained from Acros Organics. eIM (98%) and mIM (99%) were obtained from Aldrich. bIM (99%), N,N-dimethylformamide (DMF) (99.7%) and tetraethylammonium tetrafluoroborate (TEATFB) (99%) were obtained from Alfa Aesar. Acetonitrile (HPLC grade) was obtained from Fisher Scientific. Ultra-pure water (18.2 MΩ cm resistivity) was obtained from a Milli-Q Millipore Direct 8 purification unit. Methanol (≥99.8%), tributylmethylammonium methyl sulphate (TBMAMS) (≥95%) and Whatman Grade 1 Qualitative Filter Paper were obtained from Sigma Aldrich. All materials were used as received.

2.2. ZIF coating synthesis

ZIF coatings were synthesised by immersing two metal foil electrodes (geometric area ~16 cm^2 in the case of Zn and 2 cm^2 in the case of Co) held approximately 2 cm apart into a heated, de-aerated electrolyte solution containing linker. A PGSTAT302 N potentiostat (Metrohm Autolab B.V., The Netherlands) was used to apply a fixed potential difference of 2.5 V between the two metal foil electrodes for a set time, generating a coating of the ZIF on the anode surface (see Scheme 1). Table 1 contains the range of conditions used to explore the synthesis of each of the five ZIF coatings. The coated anodes were rinsed three times with methanol post synthesis to remove unreacted linker and supporting electrolyte. Material is also formed in solution in many of these syntheses but, as we are only interested in the coating, this will not be considered further.

2.3. Characterisation of ZIF coatings

The morphology and quality of the ZIF coatings were characterised on the anode surface using a FEI Quanta 200 (Environmental) Scanning Electron Microscope (E)SEM. All images were obtained at 20 kV, under low vacuum with a water vapour pressure of 0.83 Torr and utilising both Secondary and Back-scattered Electron Detectors.

The identities of the ZIF coatings were confirmed using a PANalytical X'Pert X-ray diffractometer. Powder X-ray diffraction (PXRD) patterns were obtained from ground samples of the removed coatings using Cu-Kα radiation at 40 kV and 30 mA, in the range 3–60 2θ° (with a step size of 0.017 2θ° and scan step time of 66 s) whilst spinning.

The N_2 adsorption isotherms of the ZIF coatings were obtained using a Micromeritics ASAP 2010 Volumetric Adsorption Analyser at 77 K. Ground samples of the removed coatings were first stirred in methanol overnight to remove excess linker and electrolyte from the pores and then degassed overnight at 100 °C before analysis. The BET multipoint method [72] was used on the adsorption isotherm to calculate the apparent surface areas.

2.4. Capacitance measurements and calculations

All electrochemical measurements were performed in a symmetrical two electrode configuration. Bare or ZIF-67 coated, 2 cm^2 Co foil electrodes (1.2 cm^2 active areas) and ZIF −zni, ZIF − 7, ZIF − 8 or ZIF − 14, 2 cm^2 Zn foil electrodes (1.2 cm^2 active areas) were separated by Whatman Grade 1 Qualitative Filter Paper in 1 M TEATFB in acetonitrile.

Electrochemical Impedance Spectroscopy (EIS) was performed over the frequency range 1 MHz − 200 mHz with a 10 mV RMS perturbation voltage. The experimental Nyquist plot was fitted with the standard Randles circuit.

Cyclic voltammetry was performed in the potential range 0 to 1.5 V, the step potential was 0.61 mV and the scan rate varied from 0.01 to 1 V s^{-1}.

Areal capacitance was calculated from the cyclic voltammograms using Eq. (1):

$$C = \int_{E_1}^{E_2} \frac{i(E)dE}{(E_2 - E_1)Av} \quad (1)$$

Where E_1 is the cathodic potential, E_2 is the anodic potential, i(E) is the instantaneous current, the integral gives the total power obtained from the positive and negative sweeps in the cyclic voltammogram, ν is the scan rate and A is the active electrode area of one electrode.

Galvanostatic charge-discharge was performed with the charging and discharging current densities varied between 4.2 mA cm^{-2} to 40 μA cm^{-2} and −4.2 mA cm^{-2} to −40 μA cm^{-2}

Table 1
Summary of synthesis parameters employed for the anodic growth of ZIF-4, ZIF-7, ZIF-8, ZIF-14 and ZIF-67 coatings.

	Electrodes	Linker c/mol dm^{-3}	vol% DMF/vol% H_2O	MTBAMS c/mol dm^{-3}	T/°C	t/min
ZIF-4	Zn	IM 0.15–0.30	90–25/10–75	0.06–0.12	85	15–60
ZIF-7	Zn	bIM 0.52	100/0	0.06	55	120
ZIF-8	Zn	mIM 3.00	0/100	0.06	55	60
ZIF-14	Zn	eIM 0.10–0.20	28/72	0.06–0.12	85	60
ZIF-67	Co	mIM 0.12–0.24	75/25	0.06–0.12	55–100	60–300

respectively, whilst the voltage the system was charged to varied from 1.5–0.25 V depending on the charging/discharging currents used.

Areal Capacitance was calculated from the charge-discharge curves using Eqs. (2a) and (2b):

$$C = \frac{4\frac{I}{dV/dt}}{A} \tag{2a}$$

$$C = \frac{4\frac{2I\int_{t_0}^{t_1} V(t)dt}{V'^2}}{A} \tag{2b}$$

Where I is the discharging current, dV/dt is the slope of the discharge curve, A is the active electrode area of both electrodes, t_1 is the time at the end of the discharge process, t_0 is the time at the beginning of the discharge process and V' is the voltage range of the discharge curve.

Areal energy density (W h cm^{-2}) was calculated using Eq. (3):

$$U = \frac{\frac{1}{2}CV'^2}{3600} \tag{3}$$

Where C is the areal capacitance calculated from Eq. (2) (F cm^{-2}), V' is the voltage range of the discharge curve (V) and the factor of 3600 converts W s cm^{-2} to W h cm^{-2}.

Areal power density (W cm^{-2}) was calculated using Eq. (4):

$$P = \frac{U}{t} \tag{4}$$

Where U is the areal energy density calculated using Eq. (3) (W h cm^{-2}) and t is the discharge time (hours).

3. Results and Discussion

3.1. Characterisation of ZIF electrode coatings and their syntheses

3.1.1. ZIF − 4

PXRD shows that, of the many ZIF structures reported in the literature of Zn and IM, the coating material consists of ZIF-4 (Fig. 1A). ZIF-4 is unusual in that it is not truly a "zeolitic" framework as no known zeolite adopts the same structure. The *cag* topology that it adopts (named after the chemical formula, $CaGa_2O_4$, of a mineral of the same structure) is instead found in materials such as variscite [73]. That the coating is ZIF-4 is of particular interest as it is not the densest, most thermodynamically stable Zn and IM ZIF. The most stable Zn and IM ZIF is a nonporous material with the *zni* topology (named after zinc iodide which adopts the same structure) [74,75]. As proof of the relative instability of the cag topology compared to the zni topology, heating the dry powder samples at 125 °C for 30 minutes converted the ZIF-4 coating into the non porous zni phase (Fig. 2A). It also subsequently became apparent that over longer time scales at

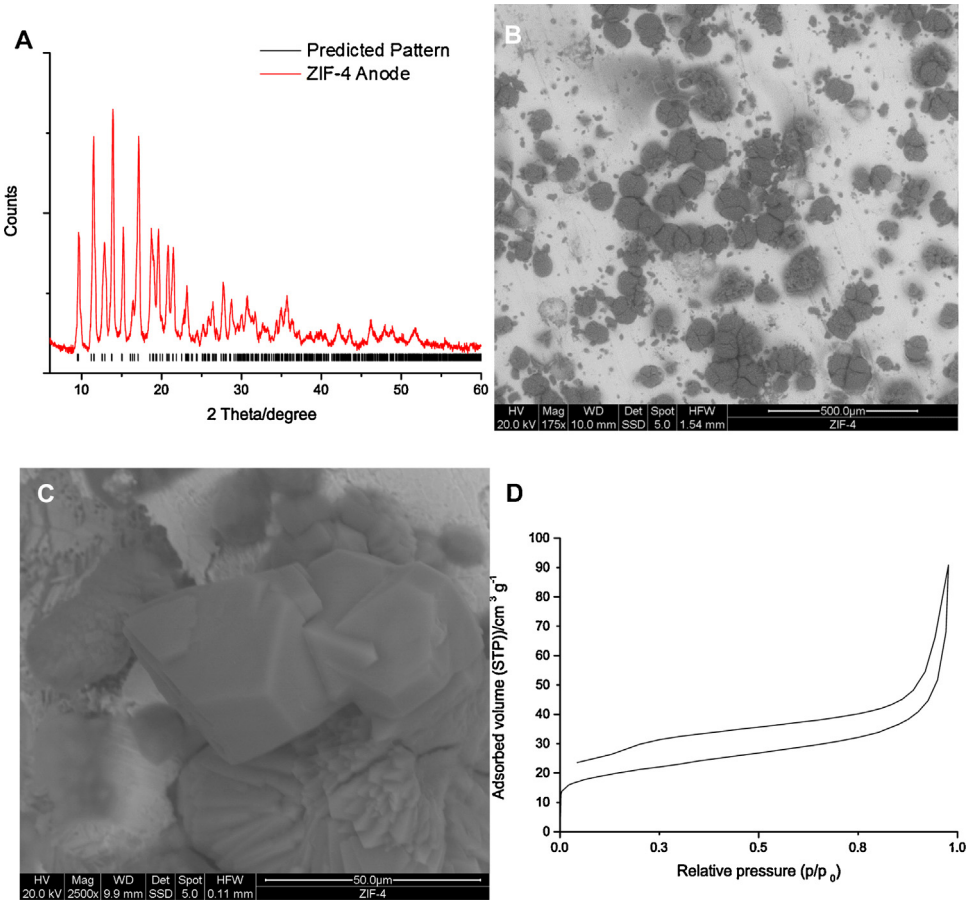

Fig. 1. PXRD (A) confirms the identity of the coating as ZIF-4 with the reflections in the experimental pattern (red) matching the predicted positions (black) [69]. SEM images (B) of the coherency of the coating of ZIF-4 on the anode and (C) the clear morphology of the constituent crystals. N_2 adsorption (D) shows the expected type I isotherm behaviour. (For interpretation of the references to colour in this figure legend, the reader is referred to the web version of this article.)

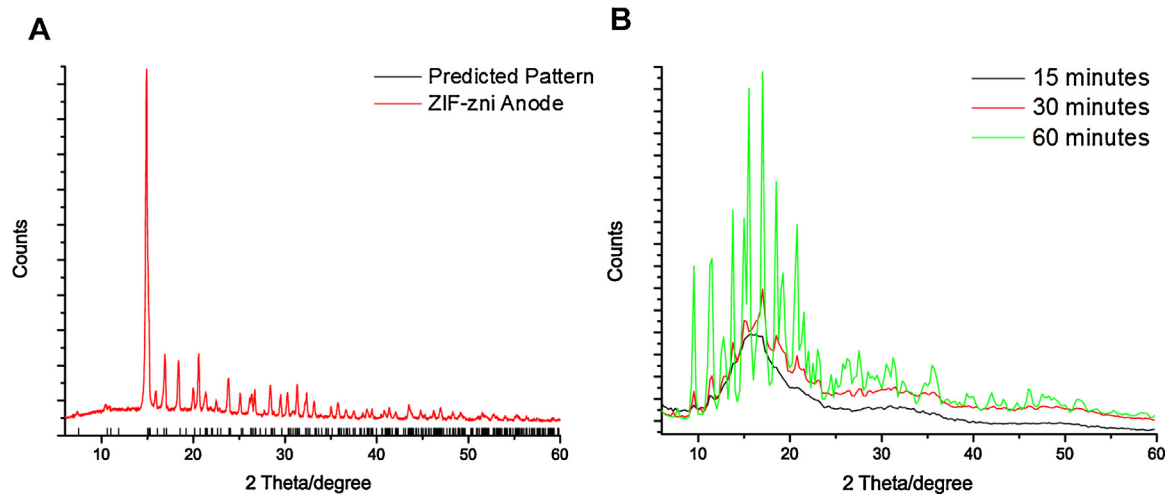

Fig. 2. PXRD (A) confirms the identity of the ZIF-4 degradation product as ZIF-zni with the reflections in the experimental pattern (red) matching the predicted positions (black) [88]. (B) The evolution of the coating material from an amorphous precursor to crystalline ZIF-4 over time is shown. (For interpretation of the references to colour in this figure legend, the reader is referred to the web version of this article.)

room temperature this conversion also occurred. Despite varying the linker concentration, the DMF:water ratio in the solvent, the supporting electrolyte concentration and reaction time, the only crystalline material obtained as a coating was ZIF-4. Under some conditions an amorphous phase was also formed. This demonstrates the importance of optimising the reaction conditions in obtaining MOF coatings. Whilst the main difference from previous literature syntheses of anodic MOF coatings was the ~50% higher reaction temperature used in order to favour crystallisation [63] the importance of reaction time, effectively metal cation concentration, is also evident. When the Zn^{2+}: IM ratio is too low (i.e. at short reaction times) an amorphous phase is seen to form, with ZIF-4 only being observed once the concentration of Zn^{2+} in solution increases (Fig. 2B).

The coherency of the coating was assessed by SEM, utilising the Z contrast provided by backscattered electrons with brighter sections corresponding to areas with little or no coating. The abundance of brighter areas observed at low magnification

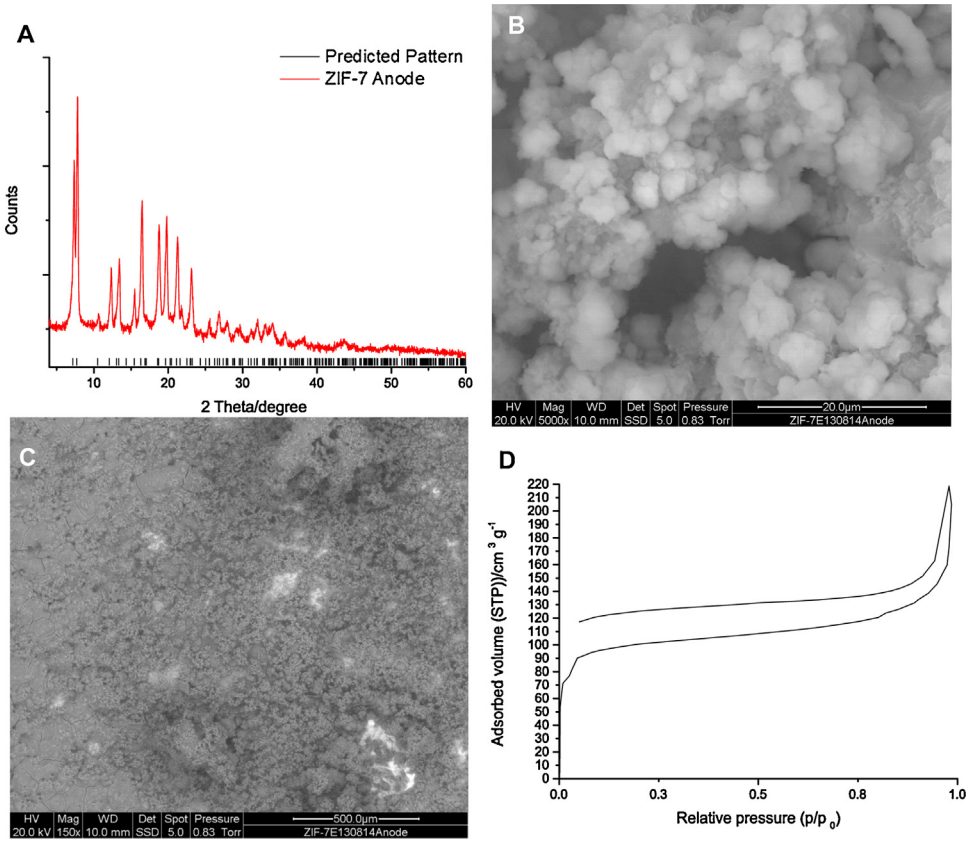

Fig. 3. PXRD (A) confirms the identity of the coating as ZIF-7 with the reflections in the experimental pattern (red) matching the predicted positions (black) [69]. SEM images of (B) the small crystal size and lack of a clear morphology of the constituent crystals and (C) the coherency of the coating of ZIF-7 on the anode. N_2 adsorption (D) shows the expected type I isotherm behaviour. (For interpretation of the references to colour in this figure legend, the reader is referred to the web version of this article.)

(Fig. 1B) demonstrates the poor quality of the coating in terms of coverage and extent of intergrowth. However some individual crystals were seen to adopt the orthorhombic dipyramidal crystal shape, at higher magnification, therefore matching the orthorhombic crystal system of variscite as seen in Fig. 1C.

The N_2 adsorption isotherm shows the expected type I behaviour and the low BET surface area of 75 $m^2 g^{-1}$ is expected for a material with only 0.2 nm pore openings (Fig. 1D) [9]. The isotherm also clearly shows evidence of hysteresis, which to the authors knowledge has only previously been observed at higher pressures [76]. There appear to be no previous reports on the adsorption behaviour of ZIF-4 over smaller pressure ranges; but with such a small pore size it is not unreasonable that hysteresis may occur at lower pressures as well.

3.1.2. ZIF − 7

PXRD confirms the identity of the coating material as ZIF − 7 (Fig. 3A). ZIF-7 adopts the sodalite (SOD) structure and is denser and more thermodynamically stable than the other Zn and bIM ZIF, ZIF-11, which adopts the RHO structure topology [69]. It is not therefore surprising that ZIF-7, rather than ZIF-11, is obtained as the coating although this represents a contrast from the formation of the kinetically favoured ZIF-4, which was obtained when using IM. The breadth of the diffraction peaks, causing the overlap of the two most intense reflections at $2\theta = 7.2^\circ$ and 7.7°, is indicative of poor crystallinity or small particle size, sub 1 μm. The SEM images indicate that poor crystallinity is the cause as they show a highly irregular coating of crystals ≥ 1 μm with no clear morphology (Fig. 3B). A lack of a clear morphology is not uncommon in the MOF crystals obtained as anode coatings and, whilst not ideal, is not necessarily prohibitive to potential applications [19,61,66].

The probable reason for the lack of a clear morphology and poor crystallinity, versus other MOF crystals obtained as anode coatings [63], is the ca. 10 times greater concentration of linker utilised in this synthesis. A much greater concentration of linker was identified as one potential method for overcoming the problem that the induction time causes for obtaining ZIF anode coatings; a significantly higher linker concentration increasing the probability of nucleation. Whilst raising the concentration of benzimidazole was successful in obtaining ZIF-7 as a coating, the side effect of increasing the nucleation rate in any crystallisation is that smaller crystals, with no clear morphology, often form as is observed to be the case here. The ZIF-7 coating is mostly coherent with some brighter areas indicating that the coverage is not complete (Fig. 3C), an issue for some potential applications but not all.

The N_2 adsorption isotherm shows the expected type I behaviour and the calculated BET surface area of 358 $m^2 g^{-1}$ matches well with literature values for material obtained by standard solvothermal synthesis [77] (Fig. 3D); demonstrating that despite the greater concentration of linker, the porosity of the coating is not compromised. As was found for ZIF-4 (Fig. 1D), the isotherm exhibits hysteresis but in this case this phenomenon has been documented previously at the same pressures as used here [78].

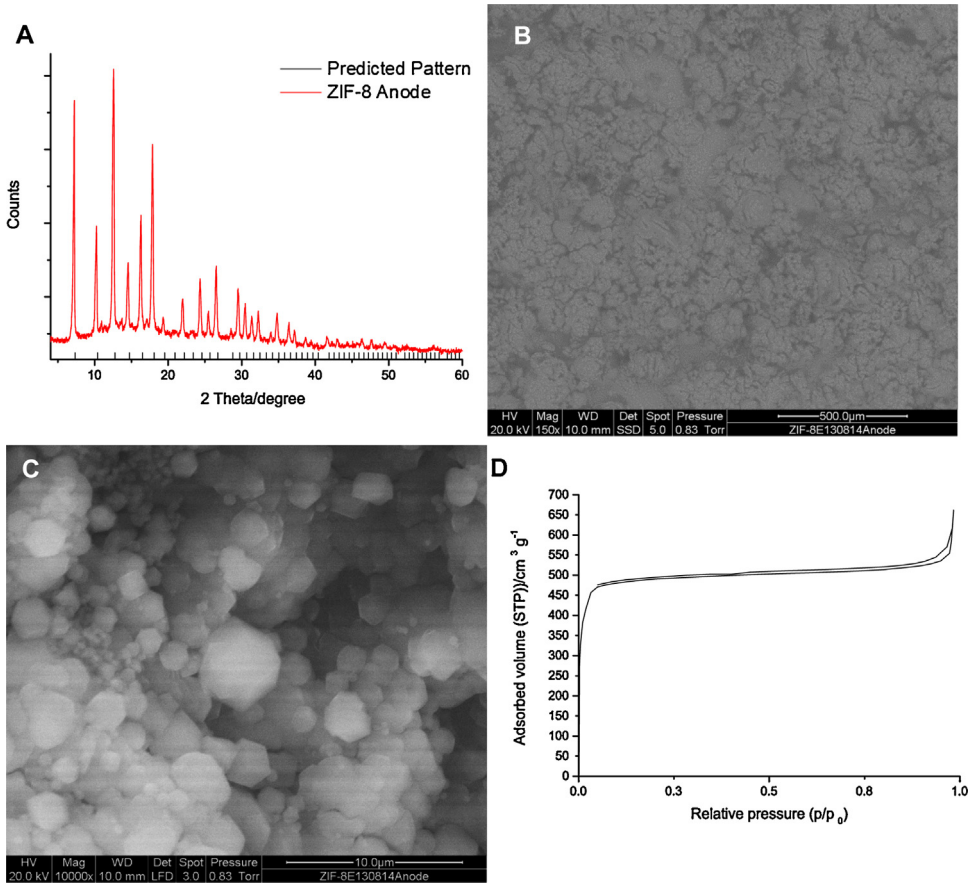

Fig. 4. PXRD (A) confirms the identity of the coating as ZIF-8 with the reflections in the experimental pattern (red) matching the predicted positions (black)[69]. SEM images of (B) the coherency of the coating of ZIF-8 over areas of many square micrometres on the anode and (C) the clear morphology of the constituent crystals. N_2 adsorption (D) shows the expected type I isotherm behaviour. (For interpretation of the references to colour in this figure legend, the reader is referred to the web version of this article.)

3.1.3. ZIF – 8

PXRD confirms that ZIF-8, which like ZIF-7 adopts the stable SOD structure, was synthesised as the coating when using Zn and mIM (Fig. 4A). This was expected as ZIF-8 is the only ZIF reported to date obtained using Zn and mIM [79]. The comparatively narrower peaks observed in the pattern, as compared to ZIF-7 (Fig. 3A), indicates a higher quality of crystal.

Initially SEM appears to indicate that the crystals constituting the coating are again small and lack clear morphology (Fig. 4B) but upon closer inspection the expected rhombic dodecahedral morphology of the ZIF-8 crystals can be observed (Fig. 4C). The coherency of the coating also appears to be better than in the case of ZIF-7, with no obvious brighter areas visible in the backscattered electron SEM image (Fig. 4B). Some potential applications for MOF coatings, such as acting as templates for electrodeposition [25], require coatings of a high coherency making this observation of interest for future work.

The N_2 adsorption isotherm shows the expected type I behaviour but the calculated BET surface area of 1730 $m^2 g^{-1}$ is around 10% lower than some of the literature values quoted for material obtained by standard solvothermal synthesis [69] (Fig. 4D). This is attributed to the even higher concentration of linker, ca. 60 times greater, used in this synthesis as compared to the anodic MOF coating synthesis in the literature [63]. This high concentration was used in combination with an aqueous electrolyte which is unusual for ZIF synthesis. This was because previous work in the literature demonstrated that a vast excess of linker in aqueous solution gave a 80% yield of ZIF-8 after only 5 minutes reaction at room temperature [80]. This synthesis clearly overcame the induction time problem and it is believed that by combining this high linker concentration, with the additional application of the mild temperature utilised in all successful anodic MOF coating syntheses reported here, a ZIF-8 coating could be obtained and the problems outlined in the literature in forming coherent coatings would be overcome [68]. Whilst this combination was clearly successful in obtaining the coating, the use of such a vast excess of linker suggests that trapped linker may be responsible for the lower than expected BET surface area. It is worth noting that the aqueous, high linker concentration electrochemical ZIF-8 synthesis appears to produce a superior product to the solvothermal method it was based upon [80]. The calculated BET surface area is 60% higher, the expected crystal morphology for ZIF-8 is more clearly observed and the reflections in the PXRD are sharper [80].

3.1.4. ZIF – 14

PXRD shows that ZIF-14 was obtained as the coating when Zn and eIM were used (Fig. 5A). ZIF-14 adopts the analcime (ANA) zeolite structure, which is slightly denser and more thermodynamically stable than the only other reported Zn and eIM structure which adopts the RHO topology [81]. There is also evidence of a second phase which is identified as ZnO [82], the presence of which is logical considering the synthesis process is reliant upon the anodic oxidation of Zn. Sharp reflections indicate, as seen with ZIF-8, high crystallinity but this is not corroborated by SEM where it is not clear whether the expected icositetrahedral crystal morphology is observed or not [83] (Fig. 5B). Lower magnification

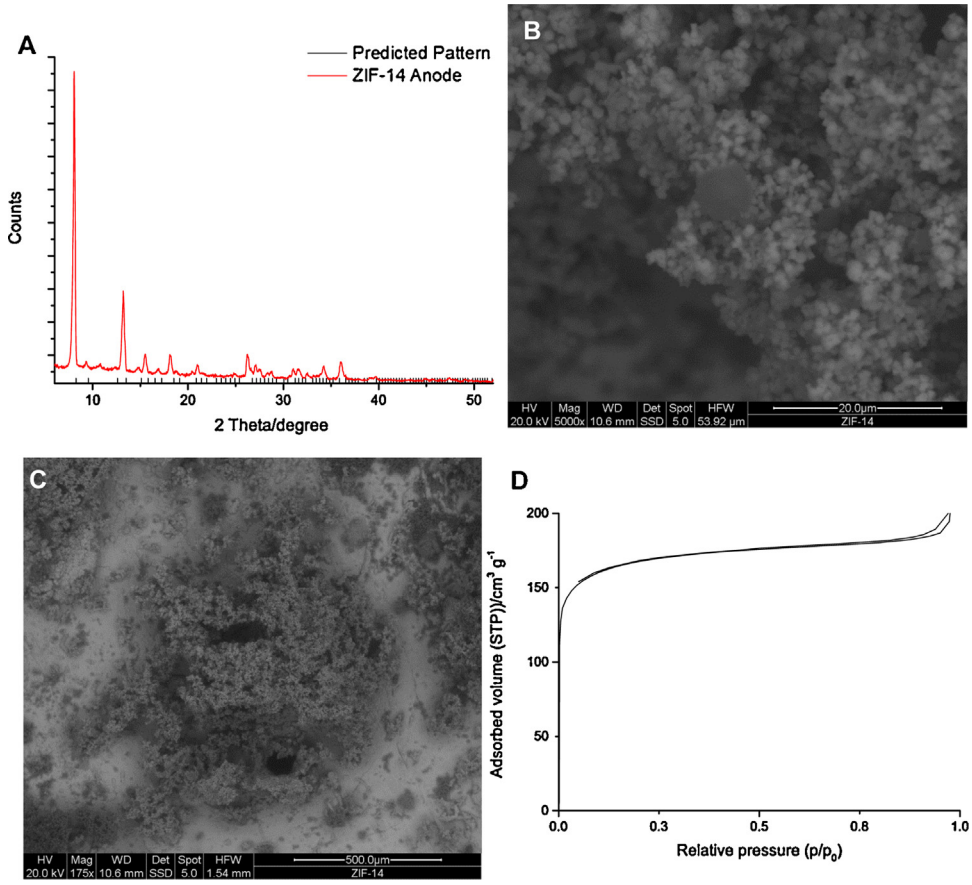

Fig. 5. PXRD (A) confirms the identity of the coating as ZIF-14 with the reflections in the experimental pattern (red) matching the predicted positions (black) [84]. SEM images of (B) the clear morphology of the constituent crystals and (C) the coherency of the coating of ZIF-14 on the anode. N_2 adsorption (D) shows the expected type I isotherm behaviour. (For interpretation of the references to colour in this figure legend, the reader is referred to the web version of this article.)

SEM images show that the coating is of a generally poor quality (Fig. 5C). It is worth noting that, alongside the elevated reaction temperature, the concentration of linker is key to obtaining the desired material as the coating. When the Zn^{2+}: eIM ratio was too high (i.e. the starting linker concentration was too low) ZnO became the predominant component of the coating, with ZIF-14 only potentially present as a very minor phase.

The porosity of ZIF-14 has been the source of recent controversy. The first paper to report on its synthesis found that it had only a very modest surface area ($\sim 29\ m^2\ g^{-1}$) [84] but very recently a surface area 20 times greater ($649–701\ m^2\ g^{-1}$) has been reported [85]. It has been suggested that this large discrepancy may be due to difficulty in fully evacuating ZIF-14, requiring higher temperatures than expected, and the slow rate at which N_2(g) penetrates the pore structure [85]. The adsorption isotherm we report here shows the type I behaviour indicative of true microporosity and the calculated BET surface area of $598\ m^2\ g^{-1}$ matches far better with the more recently reported higher values ($649–701\ m^2\ g^{-1}$) and lends support to the theory of ineffective degassing and slow analysis gas penetration (Fig. 5D).

3.1.5. ZIF − 67

PXRD confirms that ZIF-67 was obtained as the coating when Co and mIM were used (Fig. 6A). To the best of our knowledge this is the first Co MOF to be obtained as a coating via the anodic method. As the Co analogue of Zn ZIF-8, ZIF-67 also adopts the thermodynamically stable SOD structure and displays a similarly high calculated BET surface area of $1521\ m^2/g$ (Fig. 6B) which is comparable to literature values [86].

The coherency of the film appeared to be quite high (Fig. 6C) and upon closer inspection the expected rhombic dodecahedral morphology was observed (Fig. 6D)

Of the five coatings obtained ZIF-67 is potentially of most interest as a supercapacitor electrode material, as its bandgap of 1.98 eV is markedly lower than those of the other ZIFs obtained as coatings, such as ZIF-8 with a bandgap of 4.9 eV, which should give the former material a reasonable conductivity compared to the other ZIFs synthesised here [86]. EIS was performed, in order to assess the resistance of each of the five electrochemically obtained ZIF coatings.

3.2. Capacitance measurements

3.2.1. Electrochemical Impedance Spectroscopy

The Nyquist plot (Fig. 7A) demonstrates clearly that whilst the solution resistance for all five ZIF coated electrodes is similar, as evidenced by the real axis values at the high frequency intercept for each material being within $1\ \Omega$, that the charge transfer resistance of at least the four ZIF coated Zn electrodes varies significantly, as evidenced by the approximately $80\ k\Omega$ variation in the real axis values at the low frequency intercept. The Nyquist plot for ZIF-67 is only truly visible in the inset of Fig. 7A from which it is apparent that the shape of the plot is significantly different to that of the other ZIFs. The semi-circular shape of the plots for the four ZIF coated Zn electrodes shows that these materials acted as resistors over the frequency range used, with the width of the semicircle proportional to the charge transfer resistance. In contrast, the linear shape of the ZIF-67 plot makes clear that over the frequency range used ZIF-67 acted as a capacitor, with the 45°

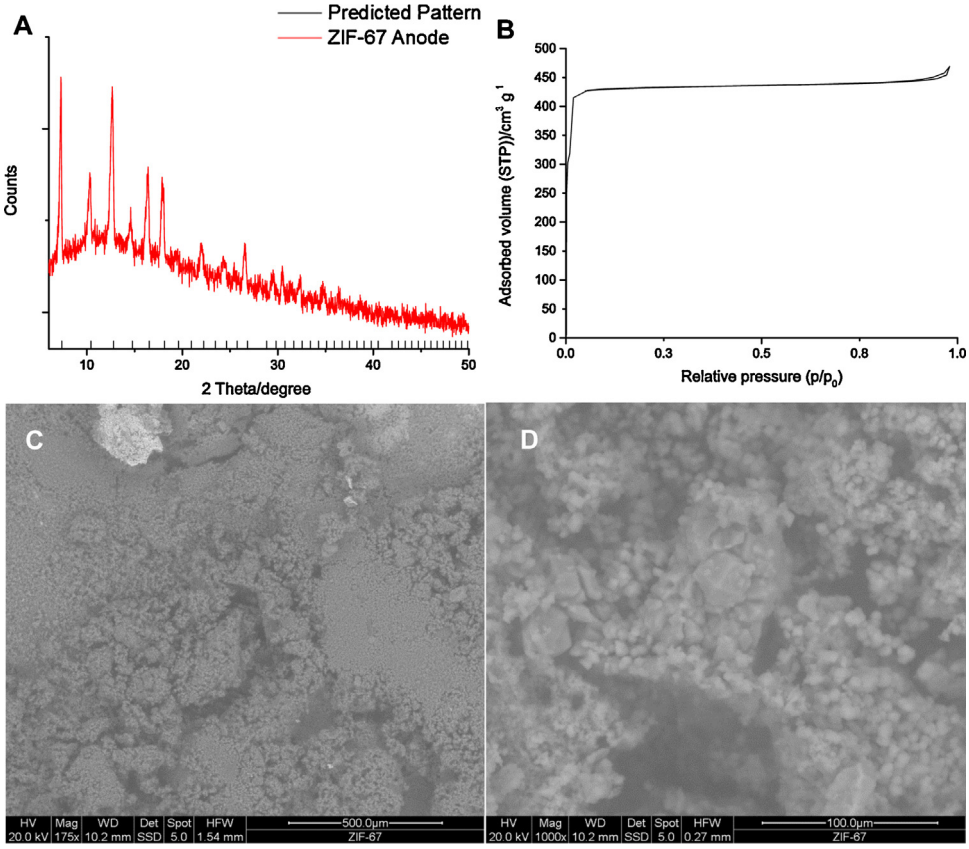

Fig. 6. PXRD (A) confirms the identity of the coating as ZIF-67 with the reflections in the experimental pattern (red) matching the predicted positions (black) [9]. N_2 adsoprtion (B) shows the expected type I isotherm behaviour. SEM images of (C) the coherency of the coating of ZIF-67 on the anode and (D) the lack of a clear morphology in the constituent crystals. (For interpretation of the references to colour in this figure legend, the reader is referred to the web version of this article.)

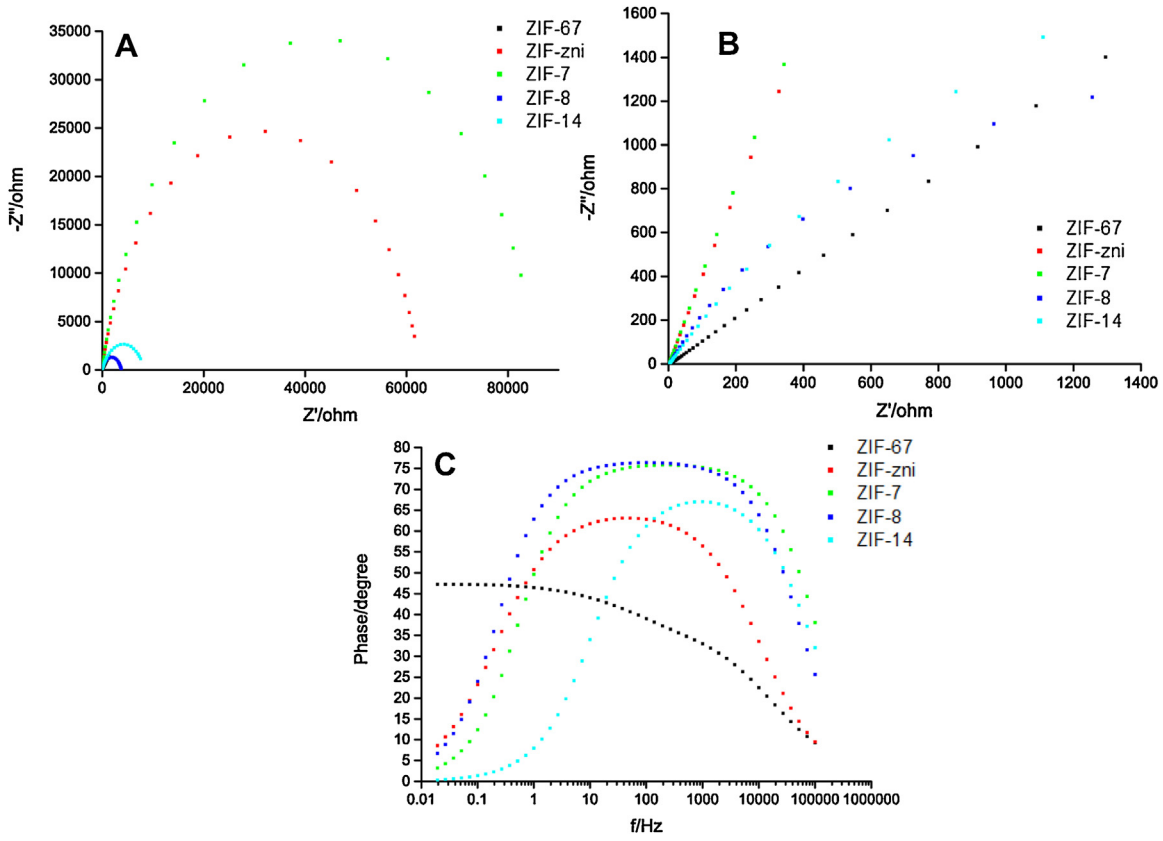

Fig. 7. Nyquist plots (A), (B) magnification of the low Z' region of (A) and Bode phase plots (C) for the five ZIF coated electrodes.

slope indicative of diffusion being a limiting process. Diffusion-limited capacitance must be due to Faradaic processes which means that any capacitance observed from ZIF-67 coated Co electrodes would primarily be from pseudo-capacitance. Fitting the data for each of the five ZIF coated electrodes with the standard Randles circuit (with the addition of a Warburg impedance for ZIF-67 to account for the pseudo-capacitance) gave the solution and charge transfer resistances listed in Table 2. It should be noted that prior to this analysis the ZIF-4 coating had degraded to ZIF – zni. As stated the solution resistance values are very similar, within 1 Ω, whilst the charge transfer resistance values vary over approximately an 80 kΩ range. As predicted ZIF-67 exhibits a significantly lower charge transfer resistance than the other four ZIFs, between approximately 200 and 4300 times.

The Bode phase plots (Fig. 7C) show a similar trend to the Nyquist plots (Fig. 7A) with the four ZIF coated Zn electrodes displaying one plot shape and the ZIF-67 coated Co electrode showing another. The shape of the ZIF – 67 plot is characteristic of a pseudo capacitor, with the initial plateau in the phase at ~45° followed by a steady decrease in phase towards 0° with increasing frequency. The frequency, which is proportional to discharge rate, at which the phase begins to decrease towards 0° is a measure of how quickly a supercapacitor electrode can operate and is dependent on the resistance of the material being used. The more resistive the material, the lower the frequency at which resistance begins to dominate over capacitance and the lower the maximum speed at which the supercapacitor can operate. The phase first begins to decrease at around 1 Hz and then decreases more rapidly after 1000 Hz, indicating the maximum speed at which the ZIF-67 based supercapacitor can operate. The shape of the plots for the four ZIF coated Zn electrodes show a different behaviour with the phase starting close to 0° at low frequency, before rising to plateau between 60° and 75° at medium frequencies and then finally decreasing again at higher frequencies. This behaviour can indicate corrosion of the underlying metal electrode [87] and could make the ZIF coated Zn electrodes unsuitable for supercapacitor electrodes, in addition to their high charge transfer resistances. Cyclic voltammetry (results not shown) is enough to confirm that Zn corrosion indeed occurs in this electrolyte system even at modest potentials, with the current from the oxidation making it impossible to make out any small potential capacitive effect from the ZIF coatings. For both these reasons only the ZIF-67 coated Co electrodes were taken forward for further capacitance analysis

Table 2
Summary of the solution R_s and charge transfer R_{CT} resistances calculated from the fitting of EIS data.

	R_s/Ω	R_{CT}/Ω
ZIF-zni	2.10	62600
ZIF-7	2.25	86100
ZIF-8	3.45	3740
ZIF-14	3.21	8320
ZIF-67	2.77	21

3.2.2. Cyclic Voltammetry

The capacitive response of bare Co electrodes (with no ZIF-67 coating) was extensively analysed by cyclic voltammetry and as expected a low capacitance was observed. Cyclic voltammetry clearly demonstrates that the ZIF-67 coated Co electrodes possess a significantly higher capacitance than bare Co electrodes. This is attributed at least in part to the extensive double layer created by

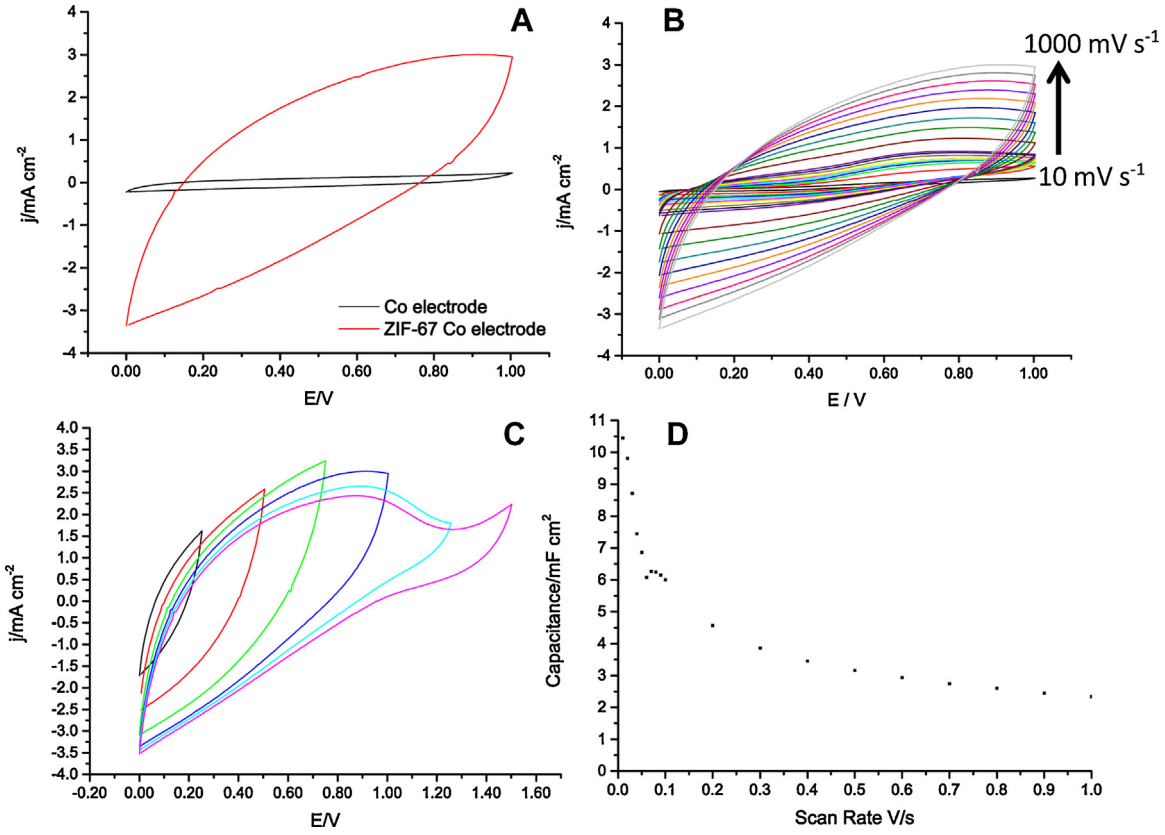

Fig. 8. Cyclic voltammetry shows the increased capacitive response due to the ZIF-67 coating at 1 V s^{-1} (A), the variation with scan rate (B), the change in charge storage mechanism from one assigned to double layer capacitance at lower potentials to a pseudo-capacitive process at higher potentials at 1 V s^{-1} (C) and the dependence of areal capacitance on scan rate (D).

the porous structure of ZIF-67 but primarily due to pseudo-capacitance originating from redox processes occurring in the ZIF-67 coating (Fig. 8A). The area inside the curve also increases with scan rate as expected (Fig. 8B). The observed increase in the slope of the cyclic voltammagrams with scan rate reflects that, despite being markedly more conductive than the other ZIFs, ZIF-67 is still a poor conductor. At higher potentials, particularly above 1 V, there is an evident Faradaic process that contributes to the observed capacititve effect (Fig. 8C). The process appears to be essentially irreversible and its absence when bare Co electrodes are used indicates that it is related to the ZIF-67 coating and not due to species present in solution, for example dissolved oxygen.

Using cyclic voltammetry data the calculated capacitance varies with scan rate as expected, with the maximum of 10.45 mF cm^{-2} at 0.01 V s^{-1} and 22% of that value retained at 1 V s^{-1} (Fig. 8D). This value is greater than that of many MOF/graphene composites [26] and seven times that of the highest reported value for "additive free" MOFs [27]. This is a crucial distinction as whilst there are many reports of much higher capacitances for various MOFs (including ZIF-67) they all, without exception, use some form of conductive additive to aid the performance of the material.

3.2.3. Galvanostatic charge – discharge

The capacitive response of ZIF-67 coated Co electrodes was also assessed using galvanostatic charge-discharge measurements in order to more accurately reflect the real working conditions of a supercapacitor device. Charge-discharge behaviour was assessed at a range of current densities over two orders of magnitude (Fig. 9A). The observed shape of the charge curves, with an initial sharp increase in potential with time followed by a slower increase up to E_{MAX}, reflects the fact that the device is resistive with the effect becoming more pronounced at lower currents. This corroborates well with the cyclic voltammetry (Fig. 8B) that showed a marked increase in the slope of the cyclic voltammograms with scan rate. Only the three highest current densities used (4.17 mA cm^{-2}, 2.92 mA cm^{-2} and 1.67 mA cm^{-2}) were sufficient to charge the device to 1.5 V, at the lower current densities of 0.42 mA cm^{-2}, 0.29 mA cm^{-2}, 0.17 mA $cm^{-2}$and 0.04 mA cm^{-2} the device was instead charged to 1.25 V, 0.75 V, 0.5 V and 0.25 V respectively. This is attributed to the still somewhat poor conductivity of ZIF-67 which for a given applied current limits the charging potential. Fitting the discharge curves (Fig. 9B) to a linear response gave fairly poor R^2 values between 0.92 and 0.98. This poor linearity is due to the pseudo-capacitive nature of the material. The capacitance was calculated from the slope of the discharge curves using Eq. (2a) to best compare with the literature. However, to more accurately assess the capacitance it was also calculated from the area under the discharge curve using Eq. (2b). The maximum capacitance calculated from Eq. (2a) was 2.61 mF cm^{-2} with a charging current density of 0.42 mA cm^{-2}, at E_{MAX} equal to 1.0 V and a discharge time of 2.5 s. The corresponding capacitance calculated from cyclic voltammetry (E_{MAX} = 1.0 V and Half cycle time = 2.5 s) was 4.09 mF cm^{-2} which compares reasonably well with a difference of ~36%. The maximum areal energy and power densities obtained of 0.42 μW h cm^{-2} and 2.08 mW cm^{-2} (at 0.42 mA cm^{-2} and 2.9 mA cm^{-2} respectively) are comparable to those of recently reported MOF- graphene and MOF-polyaniline composites [26,27]. Using Eq. (2b) the maximum areal capacitance, energy density and power density decrease to 1.15 mF cm^{-2}, 0.18 μW h cm^{-2} and 1.60 mW cm^{-2} respectively.

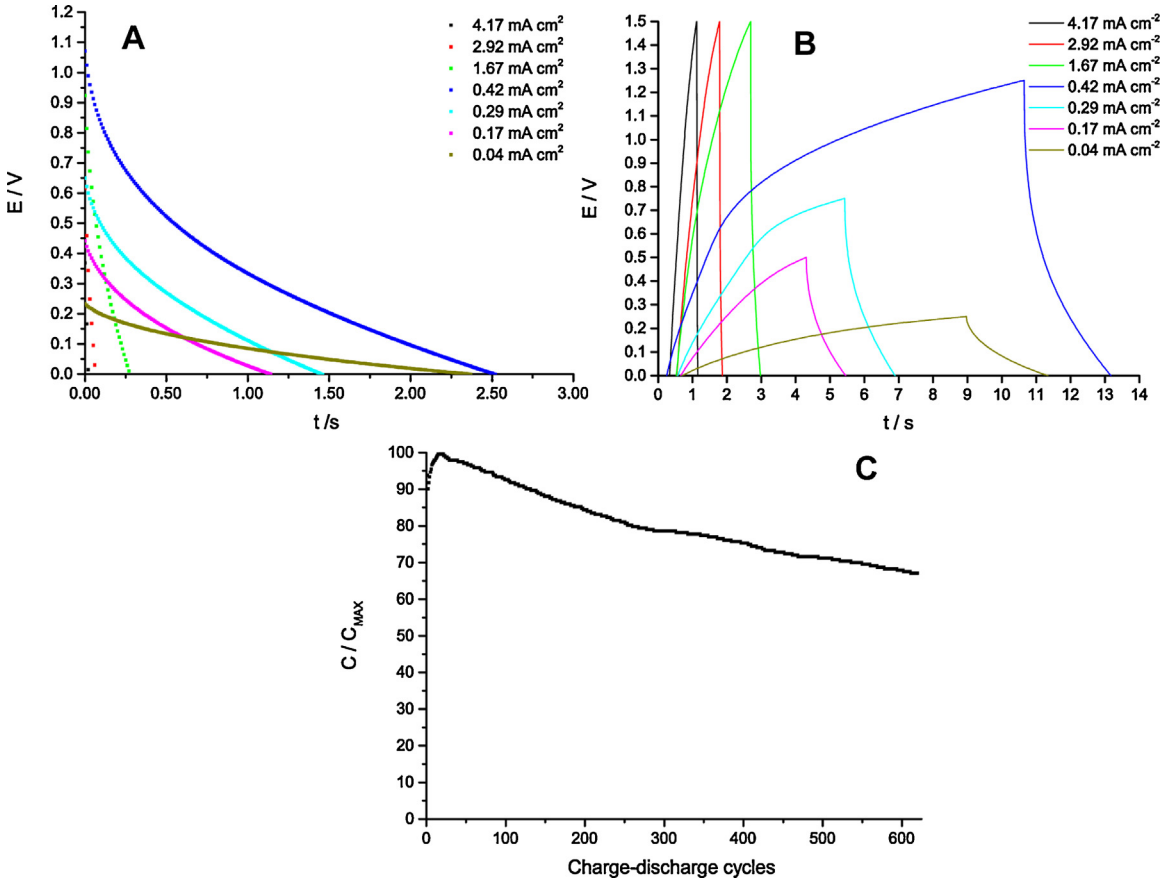

Fig. 9. Charge-discharge plots at a range of E_{MAX} and current values (A), discharge curves (B) and a plot of C/C_{MAX} against number of successive charge-discharge cycles (C).

Finally the durability of the ZIF-67 based capacitance was assessed by performing repeated charge-discharge measurements, with $E_{MAX} = 0.5$ V and $i = 0.2$ mA cm^{-2}. Capacitance as a percentage of maximum capacitance (C/C_{MAX}) was still greater than 67% after over 600 cycles (Fig. 9C). Whilst this cycling performance is worse by an order of magnitude when compared to some MOF composite materials [26,27] it is also superior by an order of magnitude to others [33]. In order to assess the cause of the decrease in capacitance with repeated cycling the used ZIF-67 coated Co electrodes were characterised again by PXRD (Fig. 10A) and SEM (Fig. 10B).

The PXRD showed that the crystalline ZIF-67 coating had mostly degraded into an amorphous material but that there was still a small amount of crystalline material present. The SEM showed an increased prevalence of brighter areas (indicative of exposed metal) compared to that seen prior to electrochemical studies (Fig. 6C); demonstrating that not only was the coating degraded but the amount of material present on the electrode had

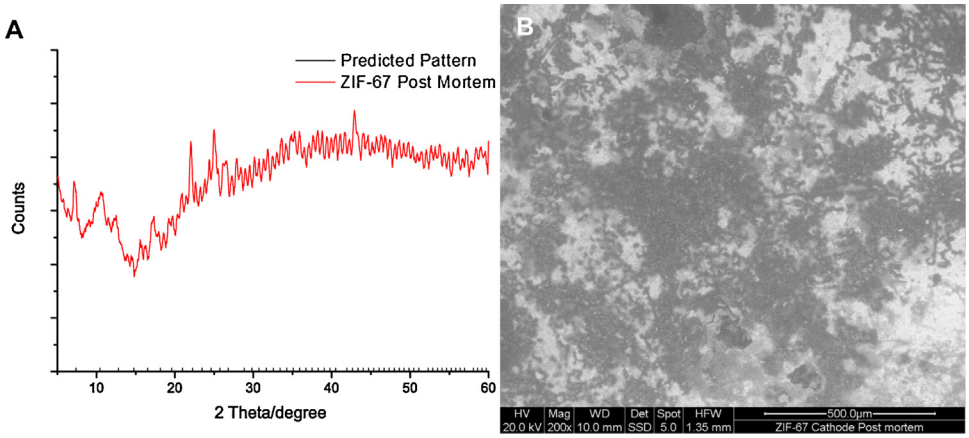

Fig. 10. PXRD (A) indicates the presence of a small amount of crystalline ZIF-67 still present in the coating after electrochemical testing with those peaks still observable in the experimental pattern (red) matching the predicted positions (black) [9]. SEM images of (B) the coherency of the coating of ZIF-67 on the electrode after electrochemical testing. (For interpretation of the references to colour in this figure legend, the reader is referred to the web version of this article.)

also decreased. Conversely it did also show that there was still a significant amount of material present, explaining how the capacitive behaviour of ZIF-67 coated Co electrodes was still retained after such extensive electrochemical testing.

4. Conclusions

Five ZIFs have been obtained as electrode coatings via the anodic growth method, four of which had not previously been obtained as coatings. These new coatings were obtained by tuning the parameters of the anodic growth method in order to favour coating growth over growth in solution. Surveying the reaction conditions in each case demonstrates that generally longer reaction times (a proxy for higher metal ion concentration), higher linker concentration and higher reaction temperature all favour coating growth over solution growth. Additionally these reaction conditions have a strong influence on the crystallinity of the coatings. These results also indicate that, for a given metal and linker combination, it is possible to obtain topologies other than the most thermodynamically stable, potentially expanding the number of structures that could be obtained as coatings via this method. Finally the potential of this additive free ZIF-67 coated Co as a supercapacitor electrode has been demonstrated and shown to outperform all reported supercapacitor materials based purely on MOFs and many MOF/graphene composite materials.

Acknowledgements

The authors would like to thank Dr. Adam Cooper and Dr. Patrick Hill for their assistance with SEM. SDW would also like to thank Dr. Eduardo Saito and Lewis Le Fevre for helpful discussions with regards to EIS and the NoWNANO DTC for funding. RAWD would like to thank the EPSRC (UK, grant references EP/K039547/1 and EP/K016954/1) for support.

References

[1] G. Ferey, Hybrid porous solids: past present, future, Chemical Society Reviews 37 (2008) 191–214.
[2] B.F. Hoskins, R. Robson, Infinite polymeric frameworks consisting of three dimensionally linked rod-like segments, Journal of the American Chemical Society 111 (1989) 5962–5964.
[3] H. Li, M. Eddaoudi, M. O'Keeffe, O.M. Yaghi, Design and synthesis of an exceptionally stable and highly porous metal-organic framework, Nature 402 (1999) 276–279.
[4] A. Henschel, K. Gedrich, R. Kraehnert, S. Kaskel, Catalytic properties of MIL-101, Chemical Communications (2008) 4192–4194.
[5] J.J. Mao, L.F. Yang, P. Yu, X.W. Wei, L.Q. Mao, Electrocatalytic four-electron reduction of oxygen with Copper (II)-based metal-organic frameworks, Electrochemistry Communications 19 (2012) 29–31.
[6] M. Sabo, A. Henschel, H. Froede, E. Klemm, S. Kaskel, Solution infiltration of palladium into MOF-5: synthesis, physisorption and catalytic properties, J. Mater. Chem. 17 (2007) 3827–3832.
[7] M.S. El-Shall, V. Abdelsayed, A. Khder, H.M.A. Hassan, H.M. El-Kaderi, T.E. Reich, Metallic and bimetallic nanocatalysts incorporated into highly porous coordination polymer MIL-101, J. Mater. Chem. 19 (2009) 7625–7631.
[8] M. Meilikhov, K. Yusenko, D. Esken, S. Turner, G. Van Tendeloo, R.A. Fischer, Metals@MOFs – Loading MOFs with Metal Nanoparticles for Hybrid Functions, Eur. J. Inorg. Chem. (2010) 3701–3714.
[9] R. Banerjee, A. Phan, B. Wang, C. Knobler, H. Furukawa, M. O'Keeffe, O.M. Yaghi, High-Throughput Synthesis of Zeolitic Imidazolate Frameworks and Application to CO2Capture, Science 319 (2008) 939–943.
[10] D. Britt, D. Tranchemontagne, O.M. Yaghi, Metal-organic frameworks with high capacity and selectivity for harmful gases, Proceedings of the National Academy of Sciences 105 (2008) 11623–11627.
[11] Q. Yang, S. Vaesen, F. Ragon, A.D. Wiersum, D. Wu, A. Lago, T. Devic, C. Martineau, F. Taulelle, P.L. Llewellyn, H. Jobic, C. Zhong, C. Serre, G. De Weireld, G. Maurin, A Water Stable Metal–Organic Framework with Optimal Features for CO_2 Capture, Angewandte Chemie International Edition 52 (2013) 10316–10320.
[12] A.R. Millward, O.M. Yaghi, Metal-Organic Frameworks with Exceptionally High Capacity for Storage of Carbon Dioxide at Room Temperature, Journal of the American Chemical Society 127 (2005) 17998–17999.
[13] Y.W. Li, R.T. Yang, Significantly enhanced hydrogen storage in metal-organic frameworks via spillover, Journal of the American Chemical Society 128 (2006) 726–727.
[14] S.R. Caskey, A.G. Wong-Foy, A.J. Matzger, Dramatic Tuning of Carbon Dioxide Uptake via Metal Substitution in a Coordination Polymer with Cylindrical Pores, Journal of the American Chemical Society 130 (2008) 10870–10871.
[15] F. Bonino, S. Chavan, J.G. Vitillo, E. Groppo, G. Agostini, C. Lamberti, P.D.C. Dietzel, C. Prestipino, S. Bordiga, Local structure of CPO-27-Ni metallorganic framework upon dehydration and coordination of NO, Chemistry of Materials 20 (2008) 4957–4968.
[16] A.C. McKinlay, B. Xiao, D.S. Wragg, P.S. Wheatley, I.L. Megson, R.E. Morris, Exceptional Behavior over the Whole Adsorption-Storage-Delivery Cycle for NO in Porous Metal Organic Frameworks, Journal of the American Chemical Society 130 (2008) 10440–10444.
[17] B. Levasseur, C. Petit, T.J. Bandosz, Reactive Adsorption of NO2 on Copper-Based Metal-Organic Framework and Graphite Oxide/Metal-Organic Framework Composites, ACS Appl. Mater. Interfaces 2 (2010) 3606–3613.
[18] S.B. Han, Y.H. Wei, C. Valente, I. Lagzi, J.J. Gassensmith, A. Coskun, J.F. Stoddart, B.A. Grzybowski, Chromatography in a Single Metal-Organic Framework (MOF) Crystal, Journal of the American Chemical Society 132 (2010) 16358–16361.
[19] N. Campagnol, T. Van Assche, T. Boudewijns, J. Denayer, K. Binnemans, D. De Vos, J. Fransaer, High pressure, high temperature electrochemical synthesis of metal-organic frameworks: films of MIL-100 (Fe) and HKUST-1 in different morphologies, J. Mater. Chem. A 1 (2013) 5827–5830.
[20] M.D. Allendorf, R.J.T. Houk, L. Andruszkiewicz, A.A. Talin, J. Pikarsky, A. Choudhury, K.A. Gall, P.J. Hesketh, Stress-induced Chemical Detection Using Flexible Metal-Organic Frameworks, Journal of the American Chemical Society 130 (2008) 14404–14405.
[21] H. Liu, H. Wang, T. Chu, M. Yu, Y. Yang, An electrodeposited lanthanide MOF thin film as a luminescent sensor for carbonate detection in aqueous solution, Journal of Materials Chemistry C 2 (2014) 8683–8690.
[22] N. Campagnol, E.R. Souza, D.E. De Vos, K. Binnemans, J. Fransaer, Luminescent terbium-containing metal-organic framework films: new approaches for the electrochemical synthesis and application as detectors for explosives, Chemical Communications 50 (2014) 12545–12547.
[23] Y. Wang, T. Chu, M. Yu, H. Liu, Y. Yang, One step cathodically electrodeposited [Tb2(BDC) 3(H2O) 4]n thin film as a luminescent probe for Cu2+ detection, Rsc Advances 4 (2014) 58178–58183.
[24] H.C. Streit, M. Adlung, O. Shekhah, X. Stammer, H.K. Arslan, O. Zybaylo, T. Ladnorg, H. Gliemann, M. Franzreb, C. Woll, C. Wickleder, Surface-Anchored MOF-Based Photonic Antennae, ChemPhysChem 13 (2012) 2699–2702.
[25] C. Lu, T. Ben, S. Xu, S. Qiu, Electrochemical Synthesis of a Microporous Conductive Polymer Based on a Metal–Organic Framework Thin Film, Angewandte Chemie International Edition 53 (2014) 6454–6458.
[26] K.M. Choi, H.M. Jeong, J.H. Park, Y.-B. Zhang, J.K. Kang, O.M. Yaghi, Supercapacitors of Nanocrystalline Metal–Organic Frameworks, ACS nano 8 (2014) 7451–7457.
[27] L. Wang, X. Feng, L. Ren, Q. Piao, J. Zhong, Y. Wang, H. Li, Y. Chen, B. Wang, Flexible Solid-State Supercapacitor Based on a Metal–Organic Framework Interwoven by Electrochemically-Deposited PANI, Journal of the American Chemical Society 137 (2015) 4920–4923.
[28] R. Díaz, M.G. Orcajo, J.A. Botas, G. Calleja, J. Palma, Co8-MOF-5 as electrode for supercapacitors, Mater. Lett. 68 (2012) 126–128.
[29] C. Liao, Y. Zuo, W. Zhang, J. Zhao, B. Tang, A. Tang, Y. Sun, J. Xu, Electrochemical performance of metal-organic framework synthesized by a solvothermal method for supercapacitors, Russ J Electrochem 49 (2013) 983–986.
[30] J. Yang, C. Zheng, P. Xiong, Y. Li, M. Wei, Zn-doped Ni-MOF material with a high supercapacitive performance, J. Mater. Chem. A 2 (2014) 19005–19010.
[31] P.C. Banerjee, D.E. Lobo, R. Middag, W.K. Ng, M.E. Shaibani, M. Majumder, Electrochemical Capacitance of Ni-Doped Metal Organic Framework and Reduced Graphene Oxide Composites: More than the Sum of Its Parts, ACS Appl. Mater. Interfaces 7 (2015) 3655–3664.
[32] R.R. Salunkhe, J. Tang, Y. Kamachi, T. Nakato, J.H. Kim, Y. Yamauchi, Asymmetric Supercapacitors Using 3D Nanoporous Carbon and Cobalt Oxide Electrodes Synthesized from a Single Metal–Organic Framework, ACS nano 9 (2015) 6288–6296.
[33] N. Campagnol, R. Romero-Vara, W. Deleu, L. Stappers, K. Binnemans, D.E. De Vos, J. Fransaer, A Hybrid Supercapacitor based on Porous Carbon and the Metal-Organic Framework MIL-100(Fe), ChemElectroChem 1 (2014) 1182–1188.
[34] V. Stavila, A.A. Talin, M.D. Allendorf, MOF-based electronic and opto-electronic devices, Chemical Society Reviews 43 (2014) 5994–6010.
[35] L. Pan, Z. Ji, X. Yi, X. Zhu, X. Chen, J. Shang, G. Liu, R.-W. Li, Metal-Organic Framework Nanofilm for Mechanically Flexible Information Storage Applications, Adv. Funct. Mater. 25 (2015) 2677–2685.
[36] S.M. Yoon, S.C. Warren, B.A. Grzybowski, Storage of Electrical Information in Metal–Organic-Framework Memristors, Angewandte Chemie International Edition 53 (2014) 4437–4441.
[37] H. Guo, G. Zhu, I.J. Hewitt, S. Qiu, Twin Copper Source Growth of Metal-Organic Framework Membrane: Cu-3(BTC)(2) with High Permeability and Selectivity for Recycling H-2, Journal of the American Chemical Society 131 (2009) 1646-.
[38] Y. Hu, X. Dong, J. Nan, W. Jin, X. Ren, N. Xu, Y.M. Lee, Metal-organic framework membranes fabricated via reactive seeding, Chemical Communications 47 (2011) 737–739.

[39] P. Falcaro, A.J. Hill, K.M. Nairn, J. Jasieniak, J.I. Mardel, T.J. Bastow, S.C. Mayo, M. Gimona, D. Gomez, H.J. Whitfield, R. Riccò, A. Patelli, B. Marmiroli, H. Amenitsch, T. Colson, L. Villanova, D. Buso, A new method to position and functionalize metal-organic framework crystals, Nat Commun 2 (2011) 237.
[40] I. Stassen, N. Campagnol, J. Fransaer, P. Vereecken, D. De Vos, R. Ameloot, Solvent-free synthesis of supported ZIF-8 films and patterns through transformation of deposited zinc oxide precursors, Crystengcomm 15 (2013) 9308–9311.
[41] Y. Mao, L. Shi, H. Huang, W. Cao, J. Li, L. Sun, X. Jin, X. Peng, Room temperature synthesis of free-standing HKUST-1 membranes from copper hydroxide nanostrands for gas separation, Chemical communications (Cambridge, England) 49 (2013) 5666–5668.
[42] M. Zhu, J.B. Jasinski, M.A. Carreon, Growth of zeolitic imidazolate framework-8 crystals from the solid-liquid interface, J. Mater. Chem. 22 (2012) 7684–7686.
[43] S. Hermes, F. Schröder, R. Chelmowski, C. Wöll, R.A. Fischer, Selective Nucleation and Growth of Metal-Organic Open Framework Thin Films on Patterned COOH/CF3-Terminated Self-Assembled Monolayers on Au(111), Journal of the American Chemical Society 127 (2005) 13744–13745.
[44] E. Biemmi, C. Scherb, T. Bein, Oriented Growth of the Metal Organic Framework Cu3(BTC) 2(H2O) 3·xH2O Tunable with Functionalized Self-Assembled Monolayers, Journal of the American Chemical Society 129 (2007) 8054–8055.
[45] A. Schoedel, C. Scherb, T. Bein, Oriented Nanoscale Films of Metal–Organic Frameworks By Room-Temperature Gel-Layer Synthesis, Angewandte Chemie International Edition 49 (2010) 7225–7228.
[46] O. Shekhah, H. Wang, S. Kowarik, F. Schreiber, M. Paulus, M. Tolan, C. Sternemann, F. Evers, D. Zacher, R.A. Fischer, C. Wöll, Step-by-Step Route for the Synthesis of Metal-Organic Frameworks, Journal of the American Chemical Society 129 (2007) 15118–15119.
[47] O. Shekhah, K. Hirai, H. Wang, H. Uehara, M. Kondo, S. Diring, D. Zacher, R.A. Fischer, O. Sakata, S. Kitagawa, S. Furukawa, C. Woll, MOF-on-MOF heteroepitaxy: perfectly oriented Zn-2(ndc)(2)(dabco)(n) grown on Cu-2(ndc)(2)(dabco)(n) thin films, Dalton Trans. 40 (2011) 4954–4958.
[48] H.K. Arslan, O. Shekhah, J. Wohlgemuth, M. Franzreb, R.A. Fischer, C. Woll, High-Throughput Fabrication of Uniform and Homogenous MOF Coatings, Adv. Funct. Mater. 21 (2011) 4228–4231.
[49] T. Ladnorg, A. Welle, S. Heißler, C. Wöll, H. Gliemann, Site-selective growth of surface-anchored metal-organic frameworks on self-assembled monolayer patterns prepared by AFM nanografting, Beilstein Journal of Nanotechnology 4 (2013) 638–648.
[50] D. Witters, S. Vermeir, R. Puers, B.F. Sels, D.E. De Vos, J. Lammertyn, R. Ameloot, Miniaturized Layer-by-Layer Deposition of Metal–Organic Framework Coatings through Digital Microfluidics, Chemistry of Materials 25 (2013) 1021–1023.
[51] R. Makiura, S. Motoyama, Y. Umemura, H. Yamanaka, O. Sakata, H. Kitagawa, Surface nano-architecture of a metal–organic framework, Nat Mater 9 (2010) 565–571.
[52] C.M. Doherty, G. Grenci, R. Riccò, J.I. Mardel, J. Reboul, S. Furukawa, S. Kitagawa, A.J. Hill, P. Falcaro, Combining UV Lithography and an Imprinting Technique for Patterning Metal-Organic Frameworks, Adv. Mater. 25 (2013) 4701–4705.
[53] P. Horcajada, C. Serre, D. Grosso, C. Boissière, S. Perruchas, C. Sanchez, G. Férey, Colloidal Route for Preparing Optical Thin Films of Nanoporous Metal–Organic Frameworks, Adv. Mater. 21 (2009) 1931–1935.
[54] Z.-Q. Li, M. Zhang, B. Liu, C.-Y. Guo, M. Zhou, Rapid fabrication of metal–organic framework thin films using in situ microwave irradiation and its photocatalytic property, Inorganic Chemistry Communications 36 (2013) 241–244.
[55] R. Ameloot, E. Gobechiya, H. Uji-i, J.A. Martens, J. Hofkens, L. Alaerts, B.F. Sels, D. E. De Vos, Direct Patterning of Oriented Metal–Organic Framework Crystals via Control over Crystallization Kinetics in Clear Precursor Solutions, Adv. Mater. 22 (2010) 2685–2688.
[56] C. Carbonell, I. Imaz, D. Maspoch, Single-Crystal Metal-Organic Framework Arrays, Journal of the American Chemical Society 133 (2011) 2144–2147.
[57] E. Bellido, S. Cardona-Serra, E. Coronado, D. Ruiz-Molina, Assisted-assembly of coordination materials into advanced nanoarchitectures by Dip Pen nanolithography, Chemical Communications 47 (2011) 5175–5177.
[58] M. Li, M. Dinca, Reductive Electrosynthesis of Crystalline Metal-Organic Frameworks (N), Journal of the American Chemical Society 133 (2011) 12926–12929.
[59] M. Li, M. Dinca, Selective Formation of Biphasic Thin Films of Metal-Organic Frameworks by Potential-Controlled Cathodic Electrodeposition, Chemical Science 5 (2014) 107–111.
[60] M. Li, M. Dincă, On the Mechanism of MOF-5 Formation under Cathodic Bias, Chemistry of Materials 27 (2015) 3203–3206.
[61] I. Stassen, M. Styles, T. Van Assche, N. Campagnol, J. Fransaer, J. Denayer, J.-C. Tan, P. Falcaro, D. De Vos, R. Ameloot, Electrochemical Film Deposition of the Zirconium Metal–Organic Framework UiO-66 and Application in a Miniaturized Sorbent Trap, Chemistry of Materials 27 (2015) 1801–1807.
[62] U. Muller, H. Putter, M. Hesse, M. Schubert, H. Wessel, J. Huff, M. Guzmann, Method for Electrochemical Production of a Crystalline Porous Metal Organic Skeleton Material, BASF Aktlengesellschaft, United States, 2006 pp. 23.
[63] R. Ameloot, L. Stappers, J. Fransaer, L. Alaerts, B.F. Sels, D.E. De Vos, Patterned Growth of Metal-Organic Framework Coatings by Electrochemical Synthesis, Chemistry of Materials 21 (2009) 2580–2582.
[64] T.R.C. Van Assche, G. Desmet, R. Ameloot, D.E. De Vos, H. Terryn, J.F.M. Denayer, Electrochemical synthesis of thin HKUST-1 layers on copper mesh, Microporous Mesoporous Mat. 158 (2012) 209–213.
[65] R. Ameloot, L. Pandey, M. Van der Auweraer, L. Alaerts, B.F. Sels, D.E. De Vos, Patterned film growth of metal-organic frameworks based on galvanic displacement, Chemical Communications 46 (2010) 3735–3737.
[66] B. Van de Voorde, R. Ameloot, I. Stassen, M. Everaert, D. De Vos, J.-C. Tan, Mechanical properties of electrochemically synthesised metal-organic framework thin films, Journal of Materials Chemistry C 1 (2013) 7716–7724.
[67] K.-Y. Cheng, J.-C. Wang, C.-Y. Lin, W.-R. Lin, Y.-A. Chen, F.-J. Tsai, Y.-C. Chuang, G.-Y. Lin, C.-W. Ni, Y.-T. Zeng, M.-L. Ho, Electrochemical synthesis, characterization of Ir-Zn containing coordination polymer, and application in oxygen and glucose sensing, Dalton Trans, 4 3 (2014) 6536–6547.
[68] A.M. Joaristi, J. Juan-Alcaniz, P. Serra-Crespo, F. Kapteijn, J. Gascon, Electrochemical Synthesis of Some Archetypical Zn2+, Cu2+, and Al3+ Metal Organic Frameworks, Cryst. Growth Des, 1 2 (2012) 3489–3498.
[69] K.S. Park, Z. Ni, A.P. Côté, J.Y. Choi, R. Huang, F.J. Uribe-Romo, H.K. Chae, M. O'Keeffe, O.M. Yaghi, Exceptional chemical and thermal stability of zeolitic imidazolate frameworks, Proceedings of the National Academy of Sciences 103 (2006) 10186–10191.
[70] N.T.T. Nguyen, H. Furukawa, F. Gándara, H.T. Nguyen, K.E. Cordova, O.M. Yaghi, Selective Capture of Carbon Dioxide under Humid Conditions by Hydrophobic Chabazite-Type Zeolitic Imidazolate Frameworks, Angewandte Chemie International Edition 53 (2014) 10645–10648.
[71] S. Yadnum, J. Roche, E. Lebraud, P. Négrier, P. Garrigue, D. Bradshaw, C. Warakulwit, J. Limtrakul, A. Kuhn, Site-Selective Synthesis of Janus-type Metal-Organic Framework Composites, Angewandte Chemie International Edition 126 (2014) 4082–4086.
[72] S. Brunauer, P.H. Emmett, E. Teller, Adsorption of gases in multimolecular layers, Journal of the American Chemical Society 60 (1938) 309–319.
[73] http://rcsr.net/nets/cag, 01/06/2015.
[74] http://rcsr.net/nets/zni, (01/06/2015).
[75] L. Bouëssel du Bourg, A.U. Ortiz, A. Boutin, F.-X. Coudert, Thermal and mechanical stability of zeolitic imidazolate frameworks polymorphs, APL Materials 2 (2014) 124110.
[76] T.D. Bennett, S. Cao, J.C. Tan, D.A. Keen, E.G. Bithell, P.J. Beldon, T. Friscic, A.K. Cheetham, Facile Mechanosynthesis of Amorphous Zeolitic Imidazolate Frameworks, Journal of the American Chemical Society 133 (2011) 14546–14549.
[77] X. Wu, M. Niknam Shahrak, B. Yuan, S. Deng, Synthesis and characterization of zeolitic imidazolate framework ZIF-7 for CO2 and CH4 separation, Microporous Mesoporous Mat. 190 (2014) 189–196.
[78] W. Cai, T. Lee, M. Lee, W. Cho, D.-Y. Han, N. Choi, A.C.K. Yip, J. Choi, Thermal Structural Transitions and Carbon Dioxide Adsorption Properties of Zeolitic Imidazolate Framework-7 (ZIF-7), Journal of the American Chemical Society 136 (2014) 7961–7971.
[79] B.R. Pimentel, A. Parulkar, E.-k. Zhou, N.A. Brunelli, R.P. Lively, Zeolitic Imidazolate Frameworks: Next-Generation Materials for Energy-Efficient Gas Separations, ChemSusChem 7 (2014) 3202–3240.
[80] Y.C. Pan, Y.Y. Liu, G.F. Zeng, L. Zhao, Z.P. Lai, Rapid synthesis of zeolitic imidazolate framework-8 (ZIF-8) nanocrystals in an aqueous system, Chemical Communications 47 (2011) 2071–2073.
[81] A. Phan, C.J. Doonan, F.J. Uribe-Romo, C.B. Knobler, M. O'Keeffe, O.M. Yaghi, Synthesis, Structure, and Carbon Dioxide Capture Properties of Zeolitic Imidazolate Frameworks, Accounts Chem. Res. 43 (2010) 58–67.
[82] F. Shi, C. Xue, Morphology and growth mechanism of novel zinc oxide nanostructures synthesized by a carbon thermal evaporation process, Crystengcomm 14 (2012) 5407–5411.
[83] W. Zhou, Microscopic study of crystal defects enriches our knowledge of materials chemistry, J. Mater. Chem. 18 (2008) 5321–5325.
[84] X.-C. Huang, Y.-Y. Lin, J.-P. Zhang, X.-M. Chen, Ligand-Directed Strategy for Zeolite-Type Metal–Organic Frameworks: Zinc(II) Imidazolates with Unusual Zeolitic Topologies, Angewandte Chemie International Edition 45 (2006) 1557–1559.
[85] D. Danaci, R. Singh, P. Xiao, P.A. Webley, Assessment of ZIF materials for CO2 capture from high pressure natural gas streams, Chemical Engineering Journal (2016).
[86] E.-X. Chen, H. Yang, J. Zhang, Zeolitic Imidazolate Framework as Formaldehyde Gas Sensor, Inorg. Chem. 53 (2014) 5411–5413.
[87] D.A. López, S.N. Simison, S.R. de Sánchez, The influence of steel microstructure on CO2 corrosion. EIS studies on the inhibition efficiency of benzimidazole, Electrochimica Acta 48 (2003) 845–854.
[88] R. Lehnert, F. Seel, Darstellung und Kristallstruktur des Mangan(II)- und Zink (II)-Derivates des Imidazols, Zeitschrift für anorganische und allgemeine Chemie 464 (1980) 187–194.